Impact of Dynamic Voltage Support and Active Power Recovery Rate on Power Swing Blocking Protection in Presence of Grid-Following PV

Meenu Jayamohan
Electrical Engineering
Indian Institute of Science
Bangalore, India
meenuj@iisc.ac.in

Sarasij Das
Electrical Engineering
Indian Institute of Science
Bangalore, India
sarasij@iisc.ac.in

Sukumar Brahma
Electrical & Computer Engineering
Clemson University
Clemson, USA
sbrahma@clemson.edu

2024 IEEE Kansas Power and Energy Conference (KPEC) | 979-8-3503-7240-3/24/$31.00 ©2024 IEEE | DOI: 10.1109/KPEC61529.2024.10676255

***Abstract*—This paper studies the impact of dynamic voltage support and active power recovery rate in a grid-connected large-scale Photovoltaic (PV) generator on Power Swing Blocking (PSB) protection used to detect Stable Power Swings (SPS). The reactive power priority (Q-priority) mode is considered during Low Voltage Ride-Through (LVRT)/High Voltage Ride-Through (HVRT). The dynamic voltage support is implemented using K-factor. The K-factor is varied to observe its impact on the power swing impedance trajectories and magnitude of the rate of change of positive-sequence impedance ($|dZ/dt|$). The impact of active power recovery rate during fault recovery on power swing trajectories and $|dZ/dt|$ are also presented. The modified IEEE-39 bus system with a Synchronous Generator (SG) replaced by a Grid-Following (GFOL) PV generator is utilized for the studies. The PV has LVRT/HVRT capabilities and complies with IEEE Standard 2800-2022. The different test cases studied are simulated using PSCAD software.**

***Index Terms*—Power swing, large-scale PV generator, K-factor, reactive power support**

I. Introduction

The introduction of Inverter-Based Resources (IBRs) like Wind Turbine Generators (WTGs) and solar Photovoltaic (PV) generators has affected the dynamic behavior of the bulk power system [1]. Fault Ride-Through (FRT) refers to the ability of generators to remain connected to the power grid during temporary voltage dips caused by faults in the transmission system. This capability is crucial for maintaining grid stability and preventing cascading outages during short-circuit events [2]. During FRT, the PV system can provide additional reactive power to the grid to maintain the voltage at its terminals. This is achieved through the dynamic voltage support or dynamic reactive power support functionality. Reactive power support is provided in proportion to the drop in voltage at the Reference Point of Applicability (RPA) using the K-factor [2]. To ensure voltage stability during grid faults, priority is given to injecting reactive power, called Q-priority. This may necessitate a reduction in active power delivery. However, existing grid codes do not mandate a specific level of active power injection during FRT events. IEEE Standard 2800-2022 specifies that the IBR should have the ability to restore the active power after a fault to its pre-fault level at an average rate of 100% by the specified active power recovery time. This is the active power recovery rate. Limiting the active power recovery rate mitigates the oscillatory behavior of IBR during the fault recovery process [2]. Existing literature has analyzed the impacts of dynamic voltage support and active power recovery rate with respect to the stability of the system [3]- [7]. However, [3]- [7] do not study the impact of K-factor or active power recovery rate on the power system protection. The transition from Synchronous Generators (SGs) to IBRs has significantly impacted power system protection functionalities as well. The addition of power electronic components and their control have impacted the operation of the relays and other protection schemes during system disturbances. The impact of LVRT of a Doubly Fed Induction Generator (DFIG) based WTG on distance relay performance has been discussed in [8]. Reference [9] addresses the challenge of protecting transmission lines connected to DFIG wind farms and proposes a modified distance protection scheme that overcomes limitations caused by DFIG behavior during faults, considering LVRT requirements. Despite their potential importance, the influence of K-factor and active power recovery rate on protection methods remains under-investigated.

Power system disturbances, such as sudden load changes, fault recovery, or generation loss, can initiate power swings. These disturbances may lead to power oscillations [10]. The Power Swing Blocking (PSB) scheme is used to prevent the maloperation of relays during Stable Power Swings (SPS). The PSB methods have also been impacted by the growing IBR penetration [11]- [16]. The impact of WTG on power swing protection has been studied in [11]. A modified Empirical Mode Decomposition (EMD) method has been proposed in [12] to detect power swings in a large-scale wind farm. Reference [13] has analyzed the efficiency of existing PSB and Out-of-Step Tripping (OST) techniques for systems with Grid-Following (GFOL) Voltage Source Converters. A non-unit protection scheme has been proposed in [14] for lines connecting PV plants, which can detect faults during power swings. A novel power swing detection method has been presented in [15] using the concentric characteristics method.

This work is funded by Tata Consulting Engineers Ltd.

979-8-3503-7240-3/24/$31.00 ©2024 IEEE

Authorized licensed use limited to: J.R.D. Tata Memorial Library Indian Institute of Science Bengaluru. Downloaded on October 22,2024 at 04:12:30 UTC from IEEE Xplore. Restrictions apply.

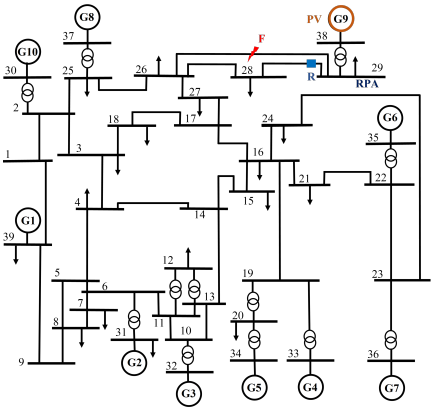

Fig. 1. Modified IEEE-39 bus transmission system

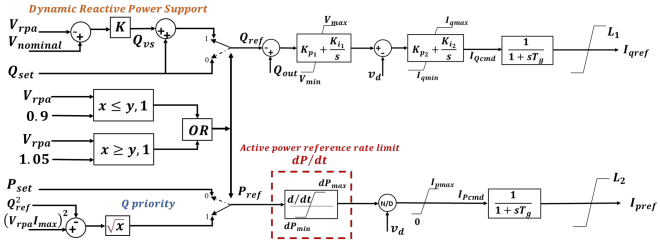

Fig. 2. Control logic for the average model of GFOL PV

Following fault removal, the dynamic behavior of inverters would be significantly influenced by both the K-factor and the active power recovery rate, which may affect the power swing characteristics. However, [11]- [15] do not analyze the impacts of K-factor or active power recovery rate.

Impedance-based methods are still the most commonly used PSB technique in commercial relays to detect power swings [17], [18]. These methods use the magnitude of the rate of change of positive-sequence impedance ($|dZ/dt|$) to differentiate power swings from fault. The existing research works do not quantify $|dZ/dt|$. Reference [16] discusses the impact of IBR integration on power swing trajectories and quantifies the $|dZ/dt|$. However, [16] does not analyze the impact of dynamic reactive power support or active power recovery rate on power swings. The goal of this work is to close the gap in the literature by providing a thorough examination of how dynamic reactive power support and the active power recovery rate affect impedance (Z) trajectories and $|dZ/dt|$ during SPS. The study has been performed for a transmission system with a large-scale GFOL PV generator. The following list includes this study's main contributions.

- The $|dZ/dt|$ seen by the relay during SPS is analyzed by varying K-factor (2-10) representing the dynamic reactive power support.
- The Z trajectory characteristics during SPS are analyzed for varying K-factor.
- Impact of active power recovery rate on $|dZ/dt|$ and Z trajectories is studied.
- The $|dZ/dt|$ and Z trajectories are studied for different steady-state reactive power references.

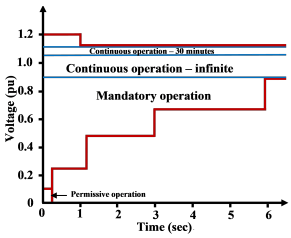

Voltage at RPA (pu)	Operating mode/response	Minimum ride-through time (s)
V>1.2	May ride-through / trip	NA
V>1.1	Mandatory operation	1
V>1.05	Continuous operation	1800
V<0.9	Mandatory operation	6
V<0.7	Mandatory operation	3
V<0.5	Mandatory operation	1.2
V<0.25	Mandatory operation	0.32
V<0.1	Permissive operation	0.32

Fig. 3. Low Voltage/ High Voltage Ride-Through characteristics

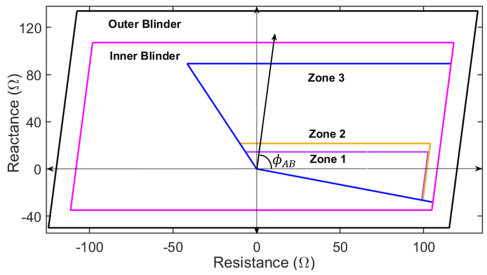

Fig. 4. Quadrilateral relay blinder setting

II. System Description

A. Test System Modeling and Control

A modified IEEE-39 bus system with the generator $G9$ replaced by a large-scale GFOL PV is used for the studies. An average model represents the large-scale GFOL PV [16], [19]. The power swing phenomenon studied is slow enough and requires only positive sequence phasor domain analysis. Hence, the average model used accurately represents PV here.

At the RPA, as shown in Fig. 1, the terminal voltage should remain between 0.9 pu and 1.05 pu under normal operating conditions. In this steady state scenario, P_{ref} is P_{set} and Q_{ref} is Q_{set}, as shown in Fig. 2. P_{set} can be provided by the Maximum Power Point Tracker (MPPT), or Power Plant Controller (PPC). The MVA rating of the PV, 870.5 MVA, is considered to be a constant for this study. Here, P_{set} and Q_{set} are set to get the required power factor (pf), keeping the MVA constant. The PV inverter operates in Q-priority mode and has LVRT/HVRT and dynamic voltage support functionalities. The LVRT/HVRT characteristics is shown in Fig. 3. Voltage support functionality, when activated during disturbance, offers reactive power support in accordance with the grid code. The voltage support feature offers additional reactive power, Q_{vs}, for change in voltage at RPA (V_{rpa}) from the nominal value ($V_{nominal}$), proportional to the K-factor [2], [20].

$$Q_{vs} = K(V_{nominal} - V_{rpa}) \tag{1}$$

K can range from 1 to 10 [20]. When voltage support gets activated in the Q-priority mode:

$$Q_{ref} = Q_{vs} + Q_{set} \tag{2}$$

$$P_{ref} = \sqrt{(V_{rpa} I_{max})^2 - Q_{ref}^2} \tag{3}$$

where, I_{max} is set to 1.2 pu to restrict the output current of the PV inverter [16].

$$I_{max} = 1.2\sqrt{(I_{Pcmd})^2 + (I_{Qcmd})^2} \tag{4}$$

where, I_{Pcmd} and I_{Qcmd} are the d-axis and q-axis current command signals, respectively. All the quantities in the above

Authorized licensed use limited to: J.R.D. Tata Memorial Library Indian Institute of Science Bengaluru. Downloaded on October 22,2024 at 04:12:30 UTC from IEEE Xplore. Restrictions apply.

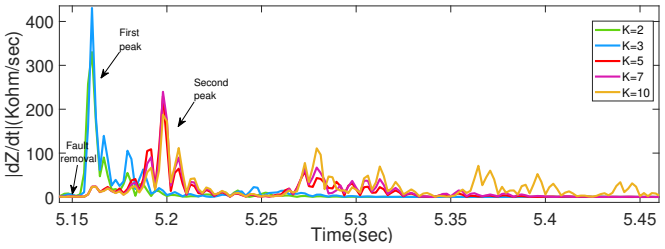

Fig. 5. $|dZ/dt|$ seen by relay R for system without dP/dt limit (pf 0.95)

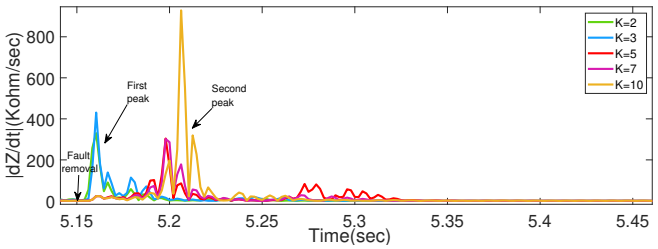

Fig. 7. $|dZ/dt|$ seen by relay R for system with dP/dt limit (pf 0.95)

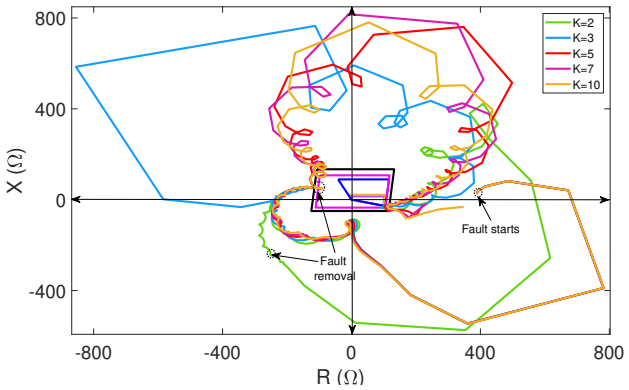

Fig. 6. Z trajectory seen by relay R for system without dP/dt limit (pf 0.95)

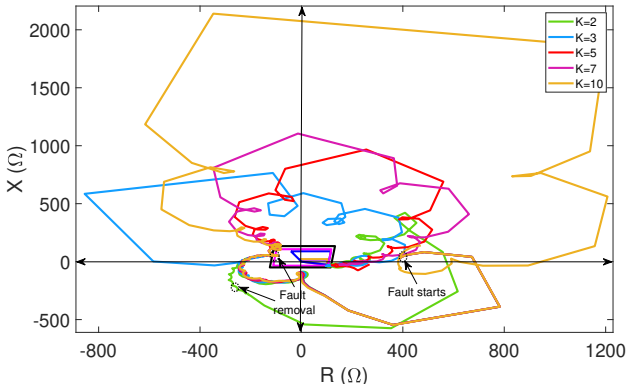

Fig. 8. Z trajectory seen by relay R for system with dP/dt limit (pf 0.95)

equations are in per unit. With a time constant of T_g = 0.02 s, the current command signals are passed through low pass filters to obtain the d-axis and q-axis current references, I_{pref} and I_{qref}, respectively. The proportional-integral (PI) control blocks employ the following parameters: for the outer Q-loop, K_{p1}=0.05 and K_{i1}=1; for the inner Q-loop, K_{p2}=1 and K_{i2}=4. The PV inverter parameters and control are as per [16].

It is to be noted that the active power recovery rate can be controlled in many ways, such as controlling the active current rate or active power reference rate during fault recovery. In this work, the active power recovery rate is controlled by limiting the active power reference rate (dP/dt), as shown in Fig. 2.

B. Power Swing Protection Settings

The quadrilateral relay and PSB setting configuration used in this study are for a conventional IEEE-39 bus system without IBR integration. As seen in Fig. 4, the two concentric blinders limit the relay characteristics, resulting in a dual quadrilateral characteristic for PSB operation. As illustrated in Fig. 4, the blinders are positioned at the relay characteristic angle, Φ_{AB}. The settings of zones and blinders are as per [16]. A PSB time delay of 30 ms (1.8 cycles) is set, as per [21], considering a maximum power swing slip rate of 4 Hz. This time delay will ensure that the worst SPS is not classified as a fault in a no-PV system.

III. Results

A SPS is generated on line 28-29, as shown in Fig. 1. A three-phase to-ground fault is created on line 26-29 at t=5 s for a duration of 0.15 s at 50% from bus 29. A fault resistance of 15 Ω is used. The fault is removed by opening the line 26-29 at t=5.15 s. As a result, power swings will be seen by relay R placed on line 28-29 near bus 29, as shown in Fig. 1. The SPS is analyzed using the $|dZ/dt|$ and the characteristics of Z trajectories seen by the relay. The $|dZ/dt|$ is estimated using the impedance and time data obtained from simulation in PSCAD, as shown in (5).

$$\left|\frac{dZ}{dt}\right| = \left|\frac{Z_{t_i} - Z_{t_{i-j}}}{t_i - t_{i-j}}\right| = \left|\frac{\Delta Z}{\Delta t}\right| \tag{5}$$

where, Δt is 2.0833 ms, $1/8^{th}$ of a cycle. The $|dZ/dt|$ and Z trajectories are analyzed for the time just after the fault removal when the SPS commences and for the region where it enters the right blinders.

*A. Test Case 1 : Q_{set}=0.3287*P_{set}, 0.95 pf*

In this study, the initial steady state reactive power reference Q_{set}=0.3287*P_{set}. This corresponds to 0.95 pf.

1) Without dP/dt Limit: The K-factor is varied from 2 to 10, and the power swing trajectory seen by relay R and $|dZ/dt|$ are observed. Unlike the slowly evolving power swings for a system with SGs, the power swings in the presence of PV move faster and, hence, have a higher $|dZ/dt|$ [16]. Also, the trajectories may enter the left blinders. On varying the K-factor, it has been observed that the $|dZ/dt|$ is highest for low K values in the first peak just after fault removal, as shown in Fig. 5. For K=2 and K=3, the $|dZ/dt|$ peak values are observed to be much higher than that for K=5, 7, and 10 in this region. The time after the first peak denotes the region where the Z trajectory takes the high-impedance path and subsequently tries to enter the right blinders/zones. The $|dZ/dt|$ is time-varying, and the Z trajectory entry into right blinders can be at different time instances for different

Authorized licensed use limited to: J.R.D. Tata Memorial Library Indian Institute of Science Bengaluru. Downloaded on October 22,2024 at 04:12:30 UTC from IEEE Xplore. Restrictions apply.

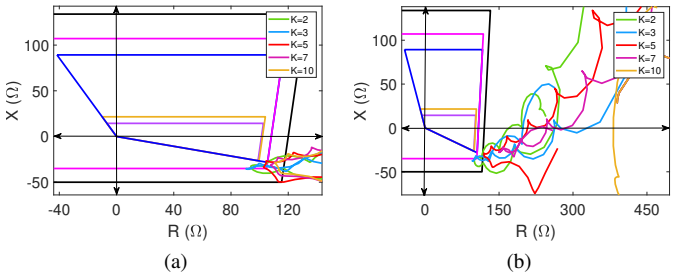

Fig. 9. Z trajectories seen by relay R (pf 0.95) (a) without (b) with dP/dt limit

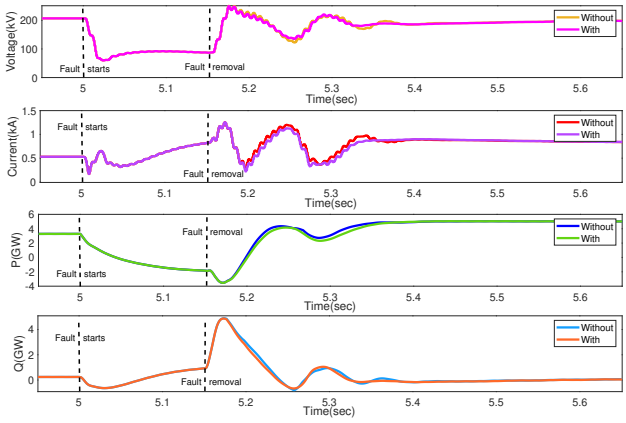

Fig. 10. (a) Voltage phasor magnitude (b) Current phasor magnitude (c) Real Power (P_R) (d) Reactive Power (Q_R) seen by relay R when K=5 for a system with and without dP/dt limit

K-factors. It can be observed that the second peak of $|dZ/dt|$ is lower than the first peak and is higher for higher K values.

On observing the Z trajectories seen by the relay R during the SPS, as shown in Fig. 6, it is clear that the trajectory does not enter the left blinders for a low value of K=2. In this case, the trajectory will not follow the high-impedance path through the top of the blinders. For cases from K= 3 to 10, the trajectories are almost similar to each other from the point of fault till the fault removal, as represented in Fig. 6. After the fault removal, the high impedance path taken by the Z trajectory varies for different values of K from 3 to 10. The reach of Z trajectories into the right blinders and zones as the K-factor is increased is shown in Fig. 9a. Here, the Z trajectories can go into the blinders and zones and cause PSB maloperation. However, higher K values have been observed to have a lower reach into the right blinders.

2) With dP/dt Limit: In this case, after fault removal, the dP/dt limit is considered as 1 pu/s. On varying the K-factor, it has been observed that the $|dZ/dt|$ values of the first peak (just after fault removal) are almost the same as that of the case without dP/dt limit, as shown in Fig. 7. The second peak of $|dZ/dt|$, occurring in the high impedance path of the trajectory, is seen to be lower than the first peak for all K values except K=10. The $|dZ/dt|$ for the second peak is observed to be higher for higher K values and decreases as K decreases. On comparison of the second peak for the cases with and without dP/dt limit, it is observed that for K values from 5 to 10, the

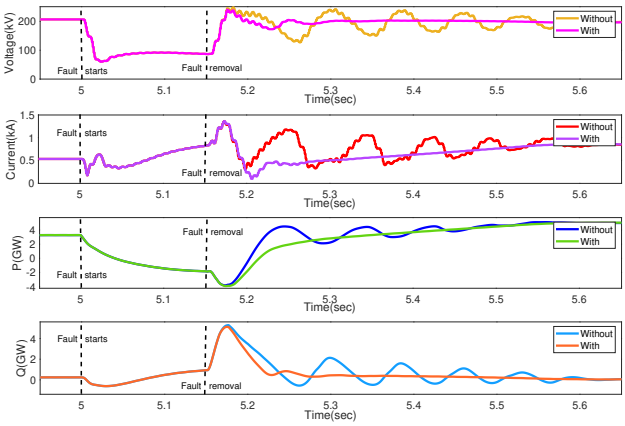

Fig. 11. (a) Voltage phasor magnitude (b) Current phasor magnitude (c) Real Power (P_R) (d) Reactive Power (Q_R) seen by relay R when K=10 for a system with and without dP/dt limit

peak is higher for the case with dP/dt limit. The comparison between Fig. 5 and Fig. 7 illustrates this. The reach of Z trajectories into the right blinders and zones as the K-factor is increased is shown in Fig. 9b. In comparison with the case without dP/dt limit, it has been observed that the reach of Z trajectories into the right blinders has decreased with the addition of the dP/dt limit. Here, the higher K values do not enter the right blinders at all.

In Fig. 8, it can also be seen that the Z trajectory does not take the high impedance path through the top of the blinder for K=2. But, after the fault removal for K values from 3 to 10, the trajectories take a very high impedance path through the top of the blinders and then try to enter the right blinders/zones. This pattern is similar to what has been found in cases where the dP/dt limit is not present. However, there is a significant difference in the expansion of the trajectories compared to the cases without dP/dt limit. The wider path taken by the Z trajectory through the top of the blinders has a much higher magnitude compared to that of the case without dP/dt limit, particularly for K values from 5 to10. This can be seen by comparing Fig. 6 and Fig. 8. As the cases with dP/dt limit have a higher $|dZ/dt|$ and larger Z trajectory in the second peak region for K=5 to 10 compared to the scenario without dP/dt limit, it can be inferred that the $|dZ/dt|$ has no strong correlation with the dP/dt alone being limited.

3) Analysis of Observations: Fig. 10, and Fig. 11 show the voltage magnitude phasor, current magnitude phasor, active power output (P_R), and reactive power output (Q_R) seen by relay R for K=5 and K=10, respectively. P_R can be seen going negative as it flows towards the load on bus 29 due to a decrease in PV real power output due to Q-priority. From Fig. 10 and Fig. 11, it can be observed that the dP/dt limit is affecting the variation of Q_R as well. Since the PV operates in Q-priority mode, the Q_R will vary so as to bring the voltage to an acceptable value. At the same time, change in Q_R is also affected by the variation of P_R, the rate of which is limited by the dP/dt limit. This dynamics between P_R and Q_R is not very significant when K is 5, as shown in Fig. 10. However, as

Authorized licensed use limited to: J.R.D. Tata Memorial Library Indian Institute of Science Bengaluru. Downloaded on October 22,2024 at 04:12:30 UTC from IEEE Xplore. Restrictions apply.

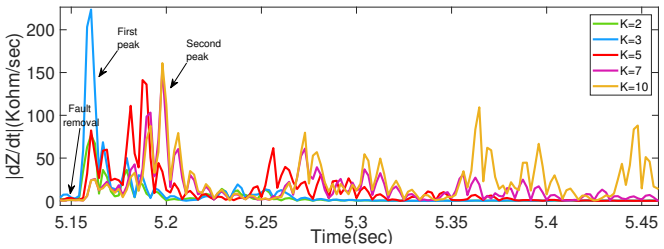

Fig. 12. $|dZ/dt|$ seen by relay R for system without dP/dt limit (pf 0.975)

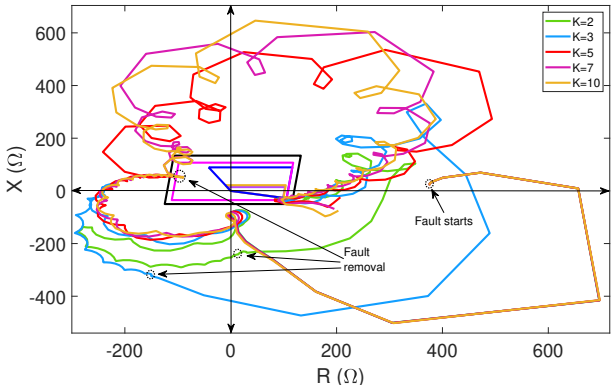

Fig. 13. Z trajectory seen by relay R for system without dP/dt limit (pf 0.975)

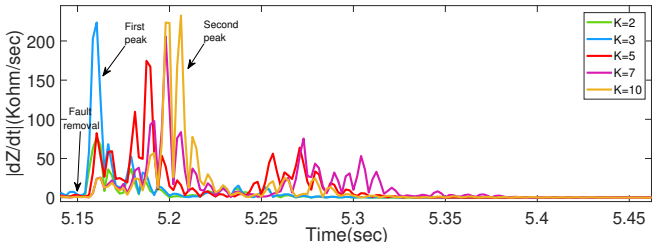

Fig. 14. $|dZ/dt|$ seen by the relay R for system with dP/dt limit (pf 0.975)

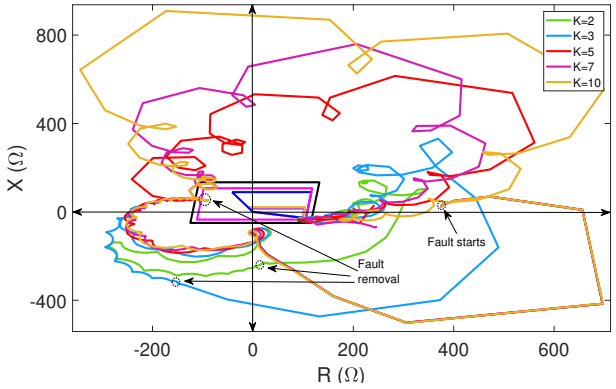

Fig. 15. Z trajectory seen by relay R for system with dP/dt limit (pf 0.975)

Fig. 11 illustrates, the dP/dt limit has a notable effect when K is 10. On observing the voltage and current phasor magnitudes, it can be seen that there is a significant variation in voltage and current after fault removal for systems with and without dP/dt limit when K= 10, but the variation is less notable when K=5. The lower current value after fault removal in the presence of dP/dt limit explains the higher impedance path taken by the Z trajectory when K=10, as shown in Fig. 11.

*B. Test case 2 : Q_{set}=0.2279*P_{set}, 0.975 pf*

Here, the reactive power reference during steady state is Q_{set}=0.2279*P_{set}, corresponding to 0.975 pf.

1) Without dP/dt Limit: The $|dZ/dt|$ has been observed to be higher for lower K values, like test case 1, for the first peak immediately after fault removal, as shown in Fig. 12. However, the peak values are much lower compared to that of test case 1. In the second peak, however, the $|dZ/dt|$ is lower compared to the first peak. Also, the $|dZ/dt|$ is higher for a higher K-factor. However, the values of the second peak of $|dZ/dt|$ for K=5 to 10 are lower compared to the second peak for test case 1.

The Z trajectories, as shown in Fig. 13, do not take the high impedance path through the top blinders when K is 2 and 3. However, for the K values from 5 to 10, the trajectory is seen to take a wider high impedance path through the top part of the blinders and subsequently enter the right blinders [16]. The Z trajectory behavior is similar to test case 1 except that the Z trajectories for K=2 and K=3 do not enter the left blinders, unlike only K=2 for test case 1. It has also been observed that the lower K-factors, from 2 to 5, have greater reach into the right blinders and zones compared to the higher K-factors, from 7 to 10. Hence, similar to test case 1, a higher K-factor prevents PSB maloperation due to entry into right blinders and zones. In comparison with the corresponding K-factor cases of test case 1, it has been observed that the extension of the Z trajectory into the right blinders/zones has increased, as shown in Fig. 16a.

2) With dP/dt Limit: In this case, after fault removal, the dP/dt limit is considered to be 1 pu/s. The $|dZ/dt|$ values of the first peak are almost the same as that of the case without the dP/dt limit, similar to test case 1, as shown in Fig. 14. In this scenario as well, the peak values are lower than those observed in test case 1. However, the $|dZ/dt|$ of the second peak is comparable to that of the first peak. But, a higher K-factor has higher $|dZ/dt|$ compared to a lower K-factor. Also, the second peak values are lower compared to that of test case 1. Similar to the case without dP/dt, here, the Z trajectories do not take a high impedance path through top blinders for K is 2 and 3, but they do so for K=5 to 10, as shown in Fig. 15. Additionally, the wider path taken by the Z trajectories for K=5 to 10 has a higher magnitude compared to that of the case without dP/dt. However, this increase is relatively small compared to that of test case 1. The Z trajectory reach into the right blinders for varying K values are shown in Fig. 16b. Similar to test case 1, the variation in Q_R depends on the voltage phasor magnitude as well as on dP/dt, and the lower current after fault removal in the presence of dP/dt limit explains the relatively higher impedance path taken by the Z trajectory for higher K-factor.

It has been observed throughout the results that for varying K-factor, the $|dZ/dt|$ corresponding to test case 2 is lower than that of test case 1. Thus, for a lower steady-state Q_{set},

Authorized licensed use limited to: J.R.D. Tata Memorial Library Indian Institute of Science Bengaluru. Downloaded on October 22,2024 at 04:12:30 UTC from IEEE Xplore. Restrictions apply.

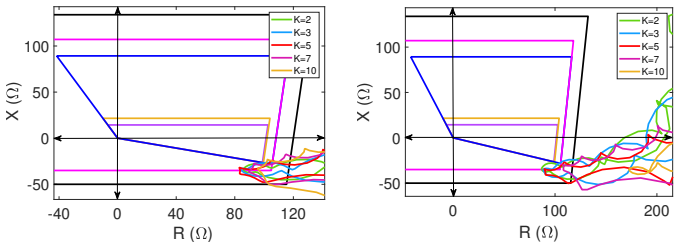

(a) (b)

Fig. 16. Z trajectories seen by relay R (pf 0.975) (a) without (b) with dP/dt limit

the $|dZ/dt|$ observed is lower than that for a higher Q_{set}. It has also been observed that for a lower Q_{set}, the Z trajectory does not enter into the left blinder for lower K values. This prevents the PSB from wrongly classifying the event as a fault. However, the reach of Z trajectories into the right blinders and zones has been observed to be greater for lower Q_{set}. This can be attributed to the relatively higher current for lower Q_{set} during blinder entry, resulting in a lower Z. For both the test cases, the Z trajectory does not enter the right blinders at all for a higher K-factor, thus reducing the chances of PSB maloperation.

IV. Summary

- The $|dZ/dt|$ values in the first peak (just after fault removal) are similar for cases with and without dP/dt limit.
- The $|dZ/dt|$ values in the second peak (during right blinder entry) is higher without dP/dt limit.
- With the addition of dP/dt limit, the high impedance region of the Z trajectories (after the fault removal) becomes larger for K-factor 5 to 10.
- Extension of the Z trajectory into the right blinders and zones is reduced with the addition of the dP/dt limit. This reduces the chances of PSB maloperation in systems with dP/dt limit.
- It is to be noted that the use of dP/dt limit doesn't guarantee lower $|dZ/dt|$ as it also depends on the dynamics of reactive power.

V. Conclusion

This study has analyzed the $|dZ/dt|$ and Z trajectories seen by relay during SPS for varying K-factor with and without active power recovery rate control, implemented using the dP/dt limit. It has been observed that the K-factor and dP/dt limit impact the Z trajectory characteristics during a power swing. The dP/dt limit is seen to result in reduced maloperation of the PSB by decreasing the extension of Z trajectories into the right blinders and zones. The dP/dt limit, however, does not ensure a reduced $|dZ/dt|$ because the $|dZ/dt|$ is also dependent on reactive power dynamics. Hence, to minimize the risk of PSB scheme maloperation, it is crucial to have a comprehensive analysis of the influence of the selected K-factor for PV dynamic reactive power support on the Z trajectory and the $|dZ/dt|$.

References

[1] K. W. Jones, et al. "Impact of Inverter Based Generation on Bulk Power System Dynamics and Short-Circuit Performance," Task Force on Short-Circuit and System Performance Impact of Inverter Based Generation, Tech. Rep. PES-TR68 (2018).

[2] "IEEE Standard for Interconnection and Interoperability of Inverter-Based Resources (IBRs) Interconnecting with Associated Transmission Electric Power Systems," in IEEE Std 2800-2022, vol., no., pp.1-180, Apr. 2022.

[3] G. Lammert et al., "Impact of Fault Ride-Through and Dynamic Reactive Power Support of Photovoltaic Systems on Short-Term Voltage Stability," 2017 IEEE Manchester PowerTech, Manchester, UK, 2017, pp. 1-6.

[4] B. Weise, "Impact of K-factor and Active Current Reduction during Fault-Ride-Through of Generating Units Connected via Voltage-Sourced Converters on Power System Stability, " *IET Renew. Power Gener.*, 9(1):25–36, 2015.

[5] Q. Hu, L. Fu, F. Ma, G. Wang, C. Liu, and Y. Ma, "Impact of LVRT Control on Transient Synchronizing Stability of PLL-Based Wind Turbine Converter Connected to High Impedance AC Grid," *IEEE Trans. Power Syst.*, vol. 38, no. 6, pp. 5445-5458, Nov. 2023.

[6] J. Hu, Q. Hu, B. Wang, H. Tang, and Y. Chi, "Small Signal Instability of PLL-Synchronized Type-4 Wind Turbines Connected to High-Impedance AC Grid During LVRT," *IEEE Trans. Energy Convers.*, vol. 31, no. 4, pp. 1676-1687, Dec. 2016.

[7] G. Lammert, D. Premm, L. D. P. Ospina, J. C. Boemer, M. Braun, and T. Van Cutsem, "Control of Photovoltaic Systems for Enhanced Short-Term Voltage Stability and Recovery," *IEEE Trans. Energy Convers.*, vol. 34, no. 1, pp. 243-254, Mar. 2019.

[8] L. He and C. C. Liu, "Impact of LVRT Capability of Wind Turbines on Distance Protection of AC Grids," 2013 IEEE PES Innovative Smart Grid Technologies Conference (ISGT), USA, 2013, pp. 1-6.

[9] X. Zhang, M. Radwan, and S. Pirooz Azad, "Modified Distance Protection of Transmission Lines Originating from DFIG-Based WPPs by Considering the Impact of Fault-Induced Rotor Frequency and LVRT Requirements," *Int. J. Electr. Power Energy Syst.*, Vol. 147, 2023.

[10] M. McDonald et al., "Power Swing and Out-of-Step Considerations on Transmission Lines," in *Proc. IEEE Power Syst. Relaying Control Committee* WG D6, 2005, vol. 6, pp. 1–59.

[11] A. Haddadi, I. Kocar, U. Karaagac, H. Gras, and E. Farantatos, "Impact of Wind Generation on Power Swing Protection," *IEEE Trans. Power Del.*, vol. 34, no. 3, pp. 1118-1128, Jun. 2019.

[12] Nazari, A.A., Razavi, F., and Fakharian, A.," A New Power Swing Detection Method in Power Systems with Large-Scale Wind Farms Based on Modified Empirical-Mode Decomposition Method," *IET Gener. Transm. Distrib.*, 17, 1204–1215 (2023).

[13] Y. Xiong, H. Wu, and X. Wang, "Efficacy Analysis of Power Swing Blocking and Out-of-step Tripping Protection for Grid-Following-VSC Systems," 8th IEEE Workshop on the Electronic Grid (eGRID), Germany, 2023, pp. 1-5.

[14] A. Chowdhury, S. Paladhi, and A. K. Pradhan, "Nonunit Protection of Parallel Lines Connecting Solar Photovoltaic Plants," *IEEE Syst. J.*, vol. 17, no. 2, pp. 2961-2970, Jun. 2023.

[15] S. Soltani, M. Abedini, and M. Sanaye-Pasand, "Power Swing Detection Using Concentric Characteristics Method: Challenges and Solutions," *IEEE Syst. J.*, vol. 18, no. 1, pp. 294-305, Mar. 2024.

[16] M. Jayamohan, S. Das, and S. Brahma, "Impedance Trajectories during Stable and Unstable Power Swings in Presence of PQ Control based PV Generations," 2023 IEEE PES General Meeting (PESGM), Orlando, FL, USA, 2023, pp. 1-5.

[17] Schneider Electric,"MiCOM P441/P442 and P444 Numerical Distance Protection Technical Guide," 2012.

[18] Siemens AG, "Distance Protection 7SA522V4.74 Manual," 2016.

[19] R. T. Elliott, A. Ellis, P. Pourbeik, J. J. Sanchez-Gasca, J. Senthil, and J. Weber, "Generic Photovoltaic System Models for WECC - A Status Report," 2015 IEEE PES General Meeting (PESGM), Denver, CO, USA.

[20] P. Adhikari, S. Brahma, and P. H. Gadde, "Source-Agnostic Time-Domain Distance Relay," *IEEE Trans. Power Del.*, vol. 37, no. 5, pp. 3620-3629, Oct. 2022.

[21] N. Fischer, G. Benmouyal, D. Hou, D. Tziouvaras, J. Byrne-Finley, and B. Smyth, "Tutorial on Power Swing Blocking and Out-of-Step Tripping," in *Proc. 39th Annu. Western Protective Relay Conf.*, Washington, 2012.

Authorized licensed use limited to: J.R.D. Tata Memorial Library Indian Institute of Science Bengaluru. Downloaded on October 22,2024 at 04:12:30 UTC from IEEE Xplore. Restrictions apply.